Energy & Environmental Science

Cite this: *Energy Environ. Sci.*, 2011, **4**, 2288

www.rsc.org/ees

PAPER

High mobility organic thin film transistor and efficient photovoltaic devices using versatile donor–acceptor polymer semiconductor by molecular design

Prashant Sonar,*[a] Samarendra P. Singh,[a] Yuning Li,*[ab] Zi-En Ooi,[a] Tae-jun Ha,[c] Ivy Wong,[a] Mui Siang Soh[a] and Ananth Dodabalapur*[ac]

Received 23rd February 2011, Accepted 11th April 2011
DOI: 10.1039/c1ee01213d

In this work, we report a novel donor–acceptor based solution processable low band gap polymer semiconductor, **PDPP–TNT**, synthesized *via* Suzuki coupling using condensed diketopyrrolopyrrole (DPP) as an acceptor moiety with a fused naphthalene donor building block in the polymer backbone. This polymer exhibits p-channel charge transport characteristics when used as the active semiconductor in organic thin-film transistor (OTFT) devices. The hole mobilities of 0.65 $cm^2 V^{-1} s^{-1}$ and 0.98 $cm^2 V^{-1} s^{-1}$ are achieved respectively in bottom gate and dual gate OTFT devices with on/off ratios in the range of 10^5 to 10^7. Additionally, due to its appropriate HOMO (5.29 eV) energy level and optimum optical band gap (1.50 eV), **PDPP–TNT** is a promising candidate for organic photovoltaic (OPV) applications. When this polymer semiconductor is used as a donor and $PC_{71}BM$ as an acceptor in OPV devices, high power conversion efficiencies (PCE) of 4.7% are obtained. Such high mobility values in OTFTs and high PCE in OPV make **PDPP–TNT** a very promising polymer semiconductor for a wide range of applications in organic electronics.

Introduction

Semiconducting polymers are important functional materials for low cost printed electronic devices, particularly for use as active materials in organic thin-film transistors (OTFTs), organic photovoltaics (OPVs), chemical sensors, *etc.*[1–5] High performance semiconducting polymers are being widely pursued aiming for improved device performance to overcome the limitations of existing organic electronics. The optoelectronic properties of polymer semiconductors are primarily governed by the conjugated blocks incorporated in the polymeric backbone. It has been well proven that the utilization of electron donating (D) and accepting (A) building blocks in the main backbone is one of the most promising and attractive strategies for making low band gap organic semiconducting polymers i.[6–8] Selection of such D–A building blocks in a conjugated backbone requires special attention paid to certain properties such as electron donating or accepting capability, planarity, chemical-electrochemical stability, and efficient tunability in electronic characteristics through side chain substitution and solid state self-assemblies. Such a D–A combination allows for band gap tuning through hybridization of the highest occupied molecular orbital (HOMO) of the donor moiety with the lowest unoccupied molecular orbital (LUMO) of the acceptor moiety. Semiconducting polymers with low band gaps with wide absorption covering from UV-vis to NIR regions are expected to be potential light harvesting materials for OPV devices.[9] A D–A system also induces intermolecular D–A interactions, leading to increased molecular ordering through self-assembly of the polymer main chains. As a result, exceptionally high mobility has been observed for certain D–A polymers in OTFT devices.[10–13] The planar pyrrolo-[3,4-*c*]pyrrole-1,4(2*H*,5*H*)-dione or diketopyrrolopyrrole (DPP)

[a]*Institute of Materials Research and Engineering (IMRE), Agency for Science, Technology, and Research (A*STAR), 3 Research Link, Singapore 117602. E-mail: sonarp@imre.a-star.edu.sg; yuning.li@uwaterloo.ca; ananth.dodabalapur@engr.utexas.edu*
[b]*Department of Chemical Engineering, University of Waterloo, 200 University Avenue West, Waterloo, Ontario, Canada N2L 3G1*
[c]*Microelectronics Research Center, The University of Texas at Austin, Austin, TX, 78758, USA*

Broader context

Donor–acceptor based solution processable polymers are an emerging class of materials for organic electronic device applications. Incorporation of fused aromatic donor and acceptor building blocks in the polymer backbone induces a strong tendency to form π–π stacks with a large overlapping area. Such materials are preferable for effective charge carrier transport through intermolecular hopping in OFET devices and also have optimum band gaps for OPV devices.

acceptor building block has been used extensively to combine with other donor building blocks such as fluorene, carbazole, phenylene, thiophene, dibenzosilole, benzodithiophene, dithienosilole, and dithienopyrrole to form various D–A copolymers.[9] DPP-based copolymers have proven to be a versatile class of materials for OTFT and OPV applications due to their high unipolar as well as ambipolar mobilities in OTFTs and high power conversion efficiencies (PCEs) in OPVs.[14–20] Recently, our group reported DPP-based donor–acceptor polymers, PDBT-*co*-TT[11] and PDQT,[12] which showed high hole mobility close to 1.0 $cm^2\ V^{-1}\ s^{-1}$. Fused aromatic rings such as thienothiophene,[10,21] benzodithiophene[22] and dithienothiophene[23] based polymer semiconductors have shown high performance in OFET devices, achieving high mobility ranging from 0.2 to 0.7 $cm^2\ V^{-1}\ s^{-1}$. Incorporation of a conjugated fused aromatic system is expected to enhance intermolecular interactions through π–π stacking and may reduce the barrier for charge carrier hopping. Optical, electrochemical, morphological and electrical properties of such organic semiconductors can be tuned by selecting coplanar D–A moieties in the polymer backbone. Interestingly, naphthalene, one of the simplest fused ring aromatic structures, has rarely been used as a building block for polymer semiconductors for OTFTs.[24,25] Naphthalene has been attached through 1,4-, 1,5- or 2,6-positions to the conjugated backbone.[26] Among them, the 2,6-attachment gives the most planar conformation to achieve extended π-conjugation. Recently, fused ring structures comprising an inner naphthalene moiety, such as naphthalene-bis(dicarboximide)[27] and naphthaodithiophene (NDT)[28] have been also used for constructing n-type and p-type polymers, which showed high electron mobility of 0.85 $cm^2\ V^{-1}\ s^{-1}$ and hole mobility of 0.54 $cm^2\ V^{-1}\ s^{-1}$ in OTFTs, respectively.

Here we report a D–A polymer using naphthalene as a donor and DPP as an acceptor, **PDPP–TNT**, and demonstrate its excellent optoelectrical performance with high hole mobility of 0.98 $cm^2\ V^{-1}\ s^{-1}$ for OTFTs and PCE of ~4.7% for OPV. Although there are several reports of using D–A polymeric semiconductors for either OFET or OPV high performance applications, there are very few D–A polymer semiconductors which have shown such high performances in both OTFT and OPV devices.

Experimental

General

All the chemicals were purchased from Strem, Acros and Sigma-Aldrich and used without further purification. All reactions were carried out using Schlenk techniques in an argon or nitrogen atmosphere with anhydrous solvents. 2,5-Dihydro-1,4-dioxo-3,6-dithienylpyrrolo [3,4-*c*]-pyrrole (DPP core) was synthesized according to the literature method.[16]

Instrumentation and characterization

^1H and ^{13}C NMR data were performed on a Bruker DPX 400 MHz spectrometer with chemical shifts referenced to residual $CHCl_3$ in $CDCl_3$. Matrix assisted laser desorption/ionization time-of-flight (MALDI-TOF) mass spectra were obtained on a Bruker Autoflex TOF/TOF instrument using dithranol as a matrix. UV-vis spectra were recorded on a Shimadzu model 2501-PC. UV-vis-NIR spectra were recorded on a Shimadzu model 2501-PC. Cyclic voltammetry experiments were performed using an Autolab potentiostat (model PGSTAT30) by Echochimie. All CV measurements were recorded in a 0.1 M tetrabutylammonium hexafluorophosphate solution in dry acetonitrile at a scanning rate of 100 $mV\ s^{-1}$. An Ag/AgCl in 3 M KCl electrode, a platinum wire, and a platinum foil were used as the reference electrode, counter electrode, and working electrode respectively. The working platinum electrode was coated with the polymer thin film by using a polymer solution in chloroform. The HOMO energy level was calculated using the equations $E_{HOMO} = E_{ox\text{-}onset} + 4.4$ eV, where $E_{ox\text{-}onset}$ is the onset potential for oxidation relative to the Ag/AgCl reference electrode. Differential scanning calorimetry (DSC) was carried out under nitrogen on a TA Instrument DSC Q100 (scanning rate of 10 °C min^{-1}). Thermogravimetric analysis (TGA) was carried out using a TA Instrument TGA Q500 at a heating rate of 10 °C min^{-1}. Atomic force microscopy (AFM) measurements were performed on polymer thin films obtained by spin coating a polymer solution in chloroform on octyltrichlorosilane (OTS)-modified p^+-Si/SiO_2. AFM images were recorded with a Nanoscope V microscope (Veeco Inc., Santa Barbara, CA) operated in tapping mode at room temperature in air, using microfabricated cantilevers (spring constant of 30 N m^{-1}). The images were recorded with 1024 pixel resolution in each direction and are shown as captured. X-Ray diffraction (XRD) patterns were recorded on spin coated thin films (~35 nm) deposited at room temperature on the OTS-modified Si/SiO_2 substrates using PANalytical X'PERT PRO system with Cu K_α (λ = 1.5418 Å) source in air. Thermal annealing was carried out on thin film samples at 100 °C and 140 °C for 15 min in nitrogen. **PDPP–TNT** samples for two-dimensional X-ray diffraction (2-D XRD) measurements were measured on the polymer flakes using Bruker AXS D8 system with Cu K_α source in air. Data were analyzed with the GADDS software.

Synthesis of 3,6-bis-(5-bromo-thiophen-2-yl)-*N,N′*-bis (2-octyldodecyl)-1,4-dioxo-pyrrolo[3,4-*c*]pyrrole (2)

In a dry three-neck 250 mL round bottom flask, 2,5-dihydro-1,4-dioxo-3,6-dithienylpyrrolo [3,4-*c*]-pyrrole (**1**) (7.0 g, 23.3 mmol) and anhydrous K_2CO_3 (9.0 g, 69.9 mmol) were dissolved in anhydrous *N*,*N*-dimethylformamide (DMF) (250 mL), and heated to 120 °C under argon for 1 h. 2-Octyldodecylbromide (25.3 g, 69.9 mmol) was then added drop-wise, and the reaction mixture was further stirred and heated overnight at 130 °C. The reaction mixture was allowed to cool down to room temperature, poured into water, and stirred for 30 min. The product was extracted with chloroform, then washed with water, and dried over $MgSO_4$. Removal of the solvent afforded the crude product which was further purified using column chromatography on silica gel using a mixture of hexane and chloroform as eluent, giving the *N*,*N′*-bis(2-octyldodecyl)-3,6-dithienyl-1,4-diketo-pyrrolo[3,4-*c*]pyrrole as a purple solid (11.0 g, 54.0%). This compound (7.0 g, 8.1 mmol) was then brominated at room temperature using slow addition of bromine (0.83 mL, 16.3 mmol) in chloroform (70 mL) in a three neck flask equipped with a stirring bar, a condenser, and a dropping funnel. The

mixture was worked up by slowly pouring the above mixture into an aqueous solution of sodium thiosulfate and stirred for an additional 30 min. The product was extracted with chloroform, successively washed with water, and dried over $MgSO_4$. Removal of the solvent afforded the crude product which was further purified using column chromatography on silica gel using a mixture of hexane and chloroform as eluent, giving the product as a dark purple solid (6.5 g, 78.0%).

^{1}H NMR (400 MHz, $CDCl_3$, δ): δ 0.86 (t, 12H), 1.10–1.47 (m, 64H), 1.88 (s, 2H), 3.98 (d, 4H), 7.52 (d, 2H), 7.22 (d, 2H), 8.63 (d, 2H).

MS (MALDI-TOF) *m/z* 1016.45 (M). Calcd. for $C_{54}H_{86}Br_2N_2O_2S_2$ = 1017.45 (M + 1).

Synthesis of 2,6-bis(4,4,5,5-tetramethyl-1,3,2-dioxabrolan-2-yl)-naphthalene (4)

2,6-Dibromo-naphthalene (**3**) (3.00 g, 10.49 mmol), bis(pinacolato)diboron (6.45 g, 25.18 mmol), $PdCl_2$(dppf) (1.85 g, 2.40 mmol), and potassium acetate (KOAc) (6.15 g, 61.52 mmol) were added in Schlenk flask and kept under vacuum for 10 min. Under an argon flow anhydrous 1,4-dioxane (40 mL) was added to the above mixture and the mixture was stirred at room temperature for 30 min before it was heated at 80 °C and stirred for 20 h. The resulting mixture was quenched by adding water and extracted with ethyl acetate (100 mL). The combined organic layer was washed with brine, dried over Na_2SO_4, and filtered. After removing the solvent, a dark red solid was obtained, which was purified by silica gel chromatography by using 3% ethyl acetate in hexane as eluent to give the title compound (**4**) as a white solid (2.5 g, 62%).

^{1}H NMR (400 MHz, $CDCl_3$): δ 8.35 (s, 2H), 7.85–7.84 (dd, 4H), 1.39 (s, 24H).

MS (MALDI-TOF) *m/z* 380.23 (M). Calcd. for $C_{22}H_{30}B_2O_4$ = 380.12.

Synthesis of PDPP–TNT

To a Schlenk flask 3,6-bis-(5-bromo-thiophen-2-yl)-*N*,*N*′-bis(2-octyldodecyl)-1,4-dioxo-pyrrolo[3,4-*c*]pyrrole (**2**) (0.350 g, 0.34 mmol), 2,6-bis(4,4,5,5-tetramethyl-1,3,2-dioxabrolan-2-yl) naphthalene (**4**) (0.130 g, 0.34 mmol), potassium carbonate (K_2CO_3) (5 mL, 2 M aqueous solution) and 2 drops of Aliquat 336 were dissolved in toluene (10 mL). The solution was purged with argon for 30 min, and then tetrakis(triphenylphosphine) palladium (20 mg, 0.017 mmol) was added. The reaction was stirred at 80 °C for 3 d. Then a solution of phenylboronic acid was added, followed by the addition of bromobenzene and stirred overnight. The resulting mixture was poured into a mixture of methanol (100 mL) and water (100 mL) and stirred overnight. The precipitated dark solid was filtered off and re-dissolved in chloroform and added drop wise to methanol (250 mL). The resulting solid was filtered off and subjected to Soxhlet extraction with methanol (24 h), acetone (24 h), and hexane (24 h), respectively. The residue was finally extracted with chloroform and precipitated again from methanol, filtered, washed with methanol, and dried *in vacuo*. 0.250 g (74% yield).

M_w/M_n (GPC) = 91 310/63 750, polydispersity index (PDI) =1.43, λ_{max} (UV-vis-near IR): 718 nm (in chloroform); 732 nm (thin film).

OTFT device fabrication and characterization

Top contact, bottom gate OTFT devices. OTFT devices were fabricated using thin films of **PDPP–TNT** (~35 nm) on octyltrichlorosilane (OTS) treated p^+-Si/SiO_2 substrates by spin-coating a polymer solution in chloroform (8 mg mL^{-1}) according to the previously reported fabrication procedure.[11] Some thin films were thermally annealed at 100–140 °C under nitrogen for 15 min. OTFT devices have a channel length (L) of 100 μm and a channel width (W) of 1 mm. Evaluation of OTFTs was carried out in a glove box under nitrogen using a Keithley 4200 parameter analyzer. The carrier mobility (μ) was calculated from the data in the saturation regime (gate voltage, V_G < source–drain voltage, V_{SD}) according to the equation: $I_{SD} = C_i\mu\,(W/2L)\,(V_G - V_T)^2$, where I_{SD} is the drain current in the saturation regime, W and L are, respectively, the transistor channel width and length, C_i is the capacitance per unit area of the gate dielectric layer, and V_T is the threshold voltage. V_T of the device is determined from the linear relationship between the square root of I_{SD} and V_G in the saturation regime of the transfer characteristics by extrapolating the linear fit to $I_{SD} = 0$.

Top contact bottom gate/bottom contact bottom gate OTFT devices. The dual gate OTFTs were fabricated using p^+-Si/SiO_2 bottom-gate electrode. Cr/Au (3 nm/50 nm) source and drain electrodes (L = 50 μm; W = 1 mm) were deposited by thermal evaporation. In order to reduce the contact resistance, Au electrodes were surface-treated with a self-assembled monolayer (SAM) of nitrobenzenethiol (NBT).[29–31] The substrates were also treated with octyltrichlorosilane (OTS) under an inert atmosphere to modify the SiO_2 gate dielectric. A thin film of **PDPP–TNT** (~35 nm) was deposited on OTS treated p^+-Si/SiO_2 substrates by spin-coating a polymer solution in chloroform (7 mg mL^{-1}) and pre-annealed at 120 °C for 30 min. The polymeric Merck dielectric (D139) as a bottom-gate insulator was spin-coated onto the **PDPP–TNT** layer for 5 s at 500 rpm in the first step and for 50 s at 1500 rpm in the second step and then was cured gradually from 25 °C to 130 °C for 1 h. This process was repeated to finish the deposition of the gate insulator. Finally, a 45 nm thick Au layer as the top-gate electrode was deposited by thermal evaporation. The device fabrication was completed with post-annealing at 140 °C for 10 h. Both the spin-coating and thermal annealing of the **PDPP–TNT** and D139 layers were performed in a glove box filled with nitrogen. OTFT devices were tested inside the glove box.

OPV device fabrication and characterization

OPV devices were fabricated on ITO glass substrates with a configuration of **Al/PDPP–TNT:PC_{71}BM/PEDOT–PSS/ITO**. The ITO glass substrates were cleaned, dried and treated with UV-ozone. A layer of PEDOT:PSS (~40 nm) was spin coated on the substrate at 1500 rpm using an aqueous solution of PEDOT:PSS and then annealed at 140 °C on a hot plate under nitrogen. The **PDPP–TNT:PC_{71}BM** blend layer was then deposited by spin-coating a solution (15 mg mL^{-1}) of **PDPP–TNT** (33 wt%) and PC_{71}BM (American Dye Source) (67 wt%) in a mixture of chloroform and *o*-dichlorobenzene (4 : 1 by volume) at 5000 rpm on top of the dried PEDOT:PSS layer. The thickness of the active

layer used in these OPV devices is around 110 nm. The sample was heated on a hot plate at 60 °C for 10 min to remove the excess solvent. An aluminium cathode was deposited by thermal evaporation through a shadow mask under a pressure of $\sim 10^{-5}$ mbar to complete the device, giving a square device area of approximately 9 mm^2.

Results and discussion

The synthetic approach to the solution processable donor–acceptor polymer **PDPP–TNT** is outlined in Scheme 1. Compound 2,5-dihydro-1,4-dioxo-3,6-dithienylpyrrolo [3,4-*c*]-pyrrole (**1**) was readily synthesized following a reported procedure,[16] which was then converted to 3,6-bis-(5-bromo-thiophen-2-yl)-*N*,*N*′-bis(2-octyldodecyl)-1,4-dioxo-pyrrolo[3,4-*c*]pyrrole (**2**) *via* alkylation and then bromination. Substitution of the branched (-octyldodecyl) group on the nitrogen atom of the DPP core is rationally designed for the better solubility purpose. Another comonomer block 2,6-bis(4,4,5,5-tetramethyl-1,3,2-dioxabrolan-2-yl)naphthalene (**4**) was obtained by reacting 2,6-dibromonaphthalene (**3**) with bis(pinacolato)diboron in the presence of $PdCl_2$(dppf) and KOAc in 1,4-dioxane.[32] Suzuki coupling polymerization of compounds **2** and **4** resulted in the polymer **PDPP–TNT** in 74% yield.

PDPP–TNT was purified by sequential Soxhlet extraction using methanol, acetone, and hexane in order to remove impurities and oligomer fractions from the bulk polymer sample. Finally the polymer was dissolved in chloroform, followed by precipitation from methanol. **PDPP–TNT** is soluble in most of the common organic solvents. The number average (M_n) and weight average molecular weight (M_w) measured by gel permeation chromatography (GPC) is 63 750 and 91 310 g mol^{-1}, respectively, at a column temperature of 40 °C with THF + chloroform as eluent and polystyrene as standards. The polydispersity index (PDI) of the copolymers is 1.43 which is calculated from the ratio of M_w and M_n. The thermal behaviour of the polymer was characterized by DSC and TGA. TGA showed a 5% weight loss at 405 °C under nitrogen, indicating the high thermal stability of **PDPP–TNT**. A bulk polymer sample was analyzed by DSC with temperatures up to 350 °C, but there were no thermal transitions observed.

The photophysical properties of **PDPP–TNT** were characterized in solution (chloroform) and in solid state (thin film on glass) by UV-vis-NIR spectroscopy. The polymer showed two broad absorption bands in the 300–500 nm and 500–800 nm regions as shown in Fig. 1. The absorption maxima (λ_{max}) in solution and solid state are located at 718 nm and 732 nm, respectively. The optical band gap (E_g^{opt}) calculated from the solid state absorption onset is ~1.50 eV, which is wider than our earlier reported polymer PDPP-*co*-TT ($E_g^{opt} \approx 1.23$ eV).[11] This could be due to the less coplanar polymer backbone and the weaker donor–acceptor interactions of **PDPP–TNT** than PDPP-*co*-TT.

The HOMO and LUMO energy levels of the **PDPP–TNT** thin film were characterized by cyclic voltammetry (CV) using 0.1 M Bu_4NPF_4 electrolyte solution in dry acetonitrile. The cyclic voltammogram of this polymer shown in Fig. 2 clearly indicates a reversible oxidation and a partially reversible reduction processes. The magnitude of the current measured during the oxidation process is higher than that of the reduction process, indicating the p-type characteristics of this polymer. The onset potential is determined from the intersection of two tangents drawn as the rising current and baseline charging current of the CV scans. The calculated HOMO value of **PDPP–TNT** is ~5.29 eV from the oxidation onset (0.89 V). Such a low HOMO value is better for oxidative stability of the polymer and also can yield high open circuit voltage (Voc) in OPV devices. The LUMO

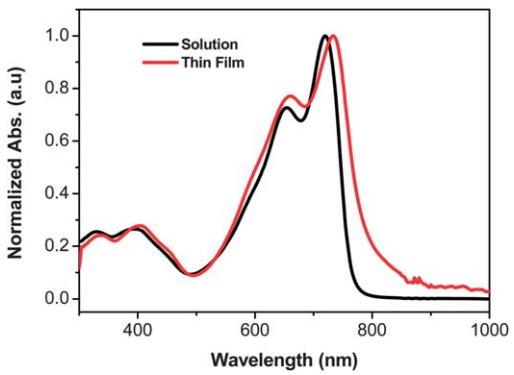

Fig. 1 Normalized UV-vis-NIR absorption spectra of **PDPP–TNT** in $CHCl_3$ solution and in the thin film on a glass substrate.

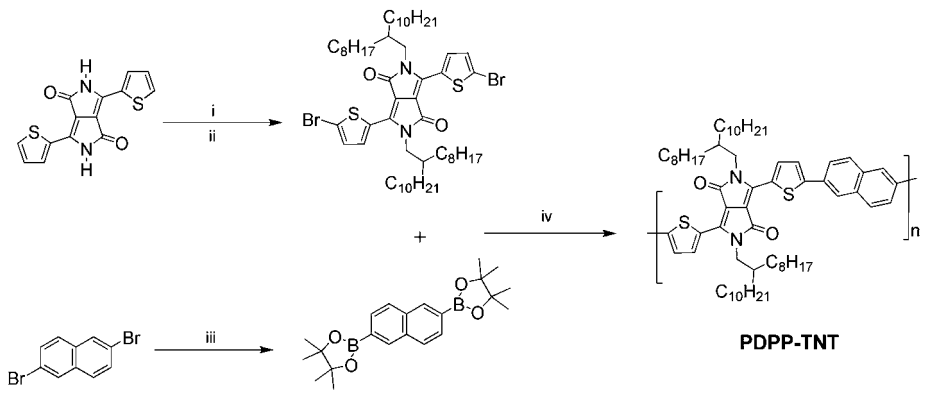

Scheme 1 Reagents and conditions: (i) K_2CO_3, 2-octl-1-dodecyl bromide, anhydrous DMF, 120–130 °C, overnight; (ii) bromine, chloroform, room temp., overnight, 78%; (iii) $PdCl_2$(dppf), 1,4-dioxane, 80 °C for 20 h, 62%; (iv) $Pd(PPh_3)_4$, aliquat 336, 2 M K_2CO_3, toluene, 80 °C for 72 h, phenylboronic acid, bromobenzene, 74%.

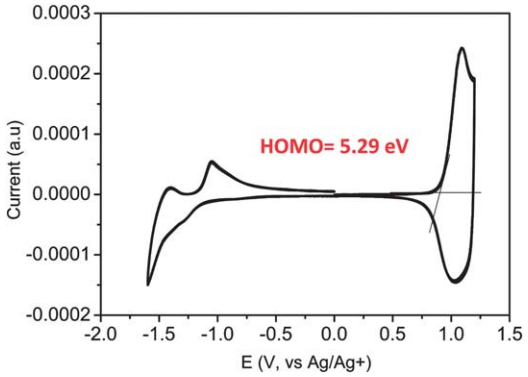

Fig. 2 Cyclic voltammogram of **PDPP–TNT** thin films on platinum electrode showing the first cathodic and anodic cycles at a scan rate 100 mV s^{-1}. The electrolyte was 0.1 M tetrabutylammonium hexafluorophosphate in anhydrous acetonitrile.

estimated from the reduction on-set potential (−1.10 V) is 4.40 – 1.00 = 3.30 eV, which is lower than the value (3.79 eV) calculated from HOMO and Eopt. The discrepancy (0.49 eV) could be due to the exciton binding energy (typically 0.4–1.0 eV) of the conjugated polymers.[33,34]

Fig. 3 shows the X-ray diffraction (XRD) patterns of the **PDPP–TNT** thin films deposited on OTS treated Si/SiO_2 substrate by spin coating. The as-spun thin film sample shows weak diffractions, indicating its poor crystallinity. Once thin films were subjected to thermal annealing at 100 °C and 140 °C, the diffraction peaks became more distinguishable. The diffraction peak at $2\theta = 4.4°$ corresponds to a *d*-spacing of 20.05 Å (100), which represents the interlayer spacing between two adjacent polymer chains. The π–π stacking diffraction peak was not observed due to blockage by the substrate.[35] Two-dimensional X-ray diffraction (2-D XRD)[22] measurements on polymer flakes were performed in order to obtain more information on the molecular ordering/arrangement. The corresponding diffractograms and their XRD images (inset pictures) obtained with the incident X-ray beam parallel/perpendicular to the polymer flakes are shown in Fig. 4a and b, respectively. In agreement with results on the thin film samples, the diffractogram of the flakes exhibited the peak (100) at $2\theta = 4.4°$ ($d = \sim 20.05$ Å). The second and third order diffraction peaks are also observed, indicating the higher crystallinity of the polymer flakes. With the incident X-ray normal to the flakes, a new diffraction peak at $2\theta = 23.20°$ is shown, which is assigned to the cofacial π–π stacking distance ($d = \sim 3.82$ Å) (Fig. 4b). The π–π stacking distance in **PDPP–TNT** (3.82 Å) is larger than that (3.71 Å) of the earlier reported PDPP-*co*-TT polymer,[11] indicating weaker intermolecular interactions of **PDPP–TNT**. A weaker intermolecular donor–acceptor interaction is due to the lesser electron donating nature of naphthalene than thieno[3,2-*b*]thiophene.

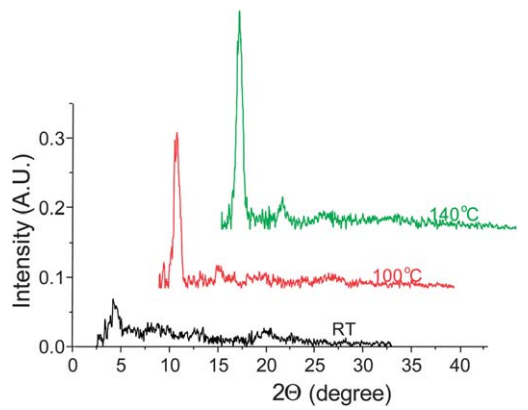

Fig. 3 X-Ray diffraction (XRD) data obtained from spin-coated **PDPP–TNT** thin films (~35 nm) on OTS modified SiO_2/Si substrates annealed at different temperatures.

Bottom-gate, top-contact OTFT devices are fabricated by spin coating a **PDPP–TNT** solution in chloroform on an OTS treated Si/SiO_2 wafer. OTS based SAM treatment controls the surface energy, induces molecular orientation and reduces the number of trapping sites for better charge transportation.[36] Gold was deposited as source and drain electrodes by thermal evaporation on top of the **PDPP–TNT** layer *via* a shadow mask. Some of the devices were pre-annealed at 100–140 °C on a hot plate for 15 min under nitrogen prior to the deposition of source/drain electrode pairs in order to study the effect of thermal annealing on charge carrier transport properties. These OTFT devices were characterized in a glove box under nitrogen using a Keithley 4200 analyzer. OTFT devices using **PDPP–TNT** as a semiconducting channel between the source and drain electrodes showed characteristic p-channel field effect performance. The hole mobility obtained from the saturation regime for the device without thermal annealing is 0.47 $cm^2\ V^{-1}\ s^{-1}$ (threshold voltage (V_T) = −17.0 V) with a current on/off ratio (I_{on}/I_{off}) of ~10^5. The device

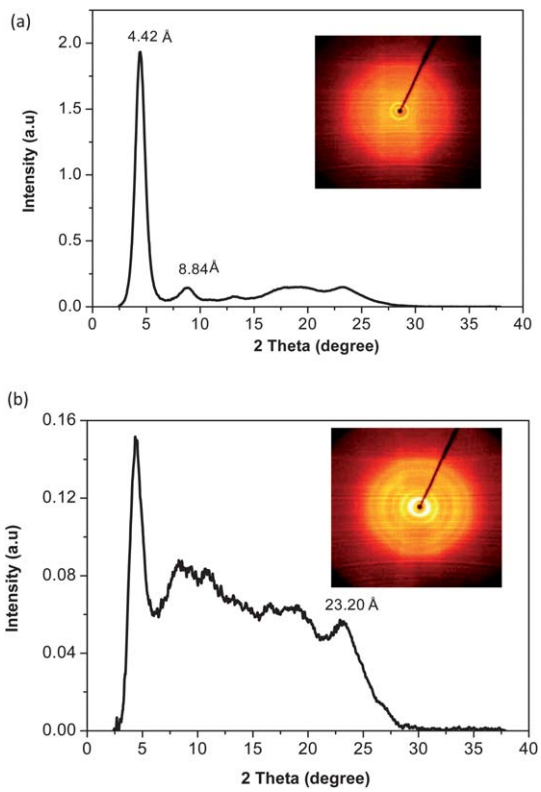

Fig. 4 2-D XRD diffractogram patterns and their 2-D XRD images (in insets) for **PDPP–TNT** film stacks with the incident X-ray parallel (a) and normal (b) to the film stacks obtained by integration of Chi (0-360) with GADDS software.

with a thin film pre-annealed at 120 °C for 15 min showed an enhanced mobility of 0.65 $cm^2 V^{-1} s^{-1}$ ($V_T = -22.0$ V) and an I_{on}/I_{off} of $\sim 10^5$. The corresponding output and transfer characteristics of the devices annealed at 120 °C for 10 min are shown in Fig. 5a and b, respectively. Pre-annealing the polymer thin film at higher temperatures (>120 °C) did not show any improvements in charge carrier mobility. To get further insights into the effect of pre-annealing on the hole mobility, atomic force microscopy (AFM) measurements were undertaken to visualize the morphological changes with respect to the increasing pre-annealing temperature. As shown in Fig. 5c, the AFM phase image of the thin film without thermal annealing shows large grains (~300 nm) with large grain boundaries. The thin film pre-annealed at 100 °C clearly shows reduced grain boundaries, but the grain size is also reduced (~200 nm). Upon further increasing the pre-annealing temperature to 140 °C, the grains become more densely packed and the grain size further decreased to ~100 nm. The decrease in the grain size with the increasing annealing temperature is rather unusual. The larger grains in the non-annealed thin films are likely rather disordered as evidenced by the thin film XRD results (Fig. 3). As the annealing temperature increases, polymer chains start to crystallize and form smaller, more densely packed crystalline grains. The large grains in the non-annealed thin film might be responsible for the relatively high mobility observed for the devices even without thermal annealing. While densely packed grains in the pre-annealed thin films are favorable for effective charge carrier transport between grains and thus fairly improved mobility is observed. However, the grain size decreases as the pre-annealing temperature increases above 120 °C, which might offset the improvements in mobility due to the reduced gaps between grains. The effect of annealing on absorption spectra of the thin film was also studied at 100 °C and 140 °C, but no significant bathochromic shift compared to room temperature processed film was observed.

PDPP–TNT is also used for the fabrication of dual gate (top contact bottom gate/bottom contact bottom gate) OTFT devices, in which two different gate dielectrics have been used in a single device. The device geometry is shown in Fig. 6a. In such a device two accumulation channels can be formed due to isolation of semiconducting material by two gate insulators and the channel conductance can be controlled by applying voltages at two gate electrodes independently. The corresponding output and the saturation mobility *versus* gate voltage characteristics are shown in Fig. 6a and b, respectively, for the best devices. These devices exhibited higher hole mobility around 0.98 $cm^2 V^{-1} s^{-1}$ for pre-annealed thin film at 120 °C with lower leakage current and high I_{on}/I_{off} of $\sim 2 \times 10^7$. Such high mobility and current on/off ratio observed in these devices are due to the effects of the NBT (nitrobenzenethiol) SAM treatment of the source–drain electrodes (see Experimental) and dual-gate device geometry which reduces the contact resistance and enhances charge carrier injection in channel. It is well proven that due to SAM treatment

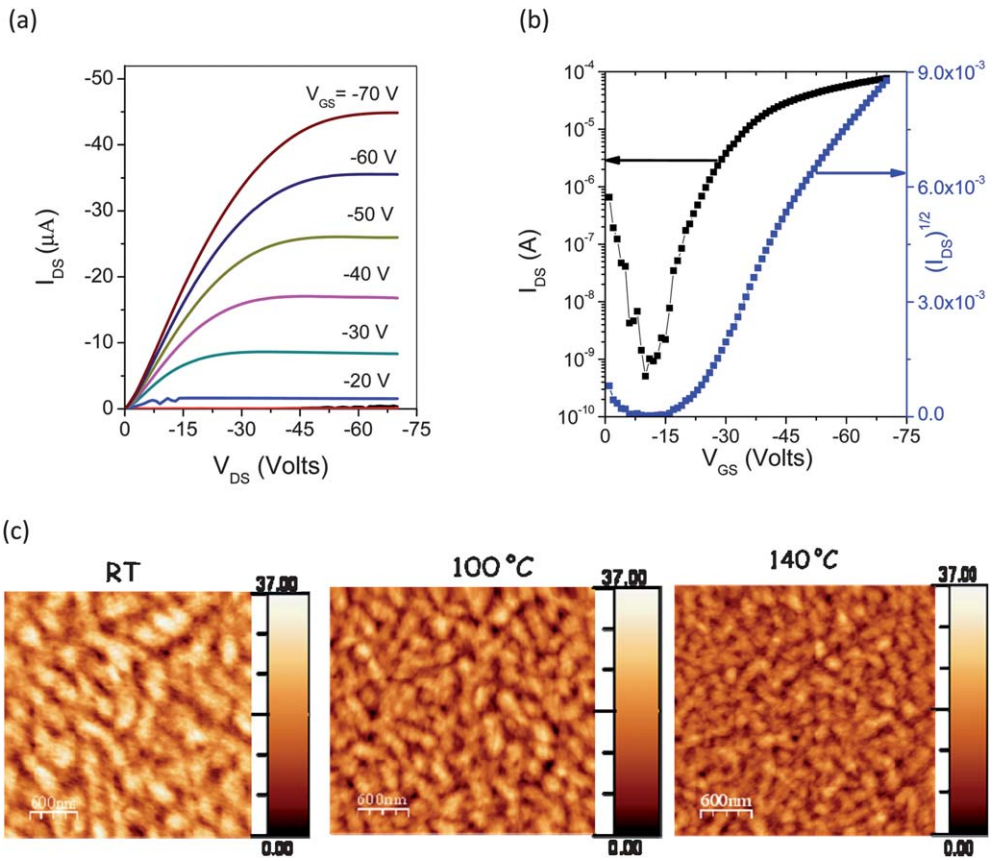

Fig. 5 (a) Output (V_{DS} *vs.* I_{DS}) and (b) transfer characteristics (V_{GS} *vs.* I_{DS}) of an OTFT (L = 100 μm; W = 1000 μm) on OTS treated p^+-Si/SiO_2 substrate with 120 °C pre-annealed **PDPP–TNT** thin film (c) AFM phase images of **PDPP–TNT** thin films without annealing (room temperature) and annealed at 100 °C and 140 °C on OTS treated p^+-Si/SiO_2 substrates.

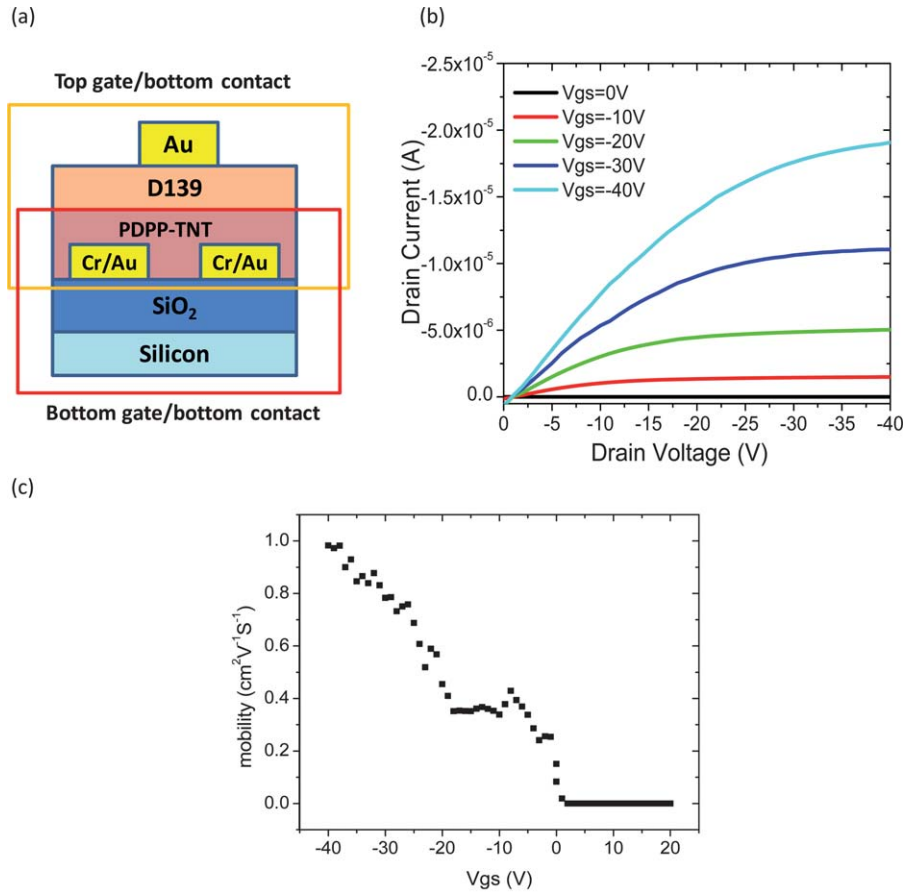

Fig. 6 (a) The cross section of a dual gate based OTFT using **PDPP–TNT**, (b) output characteristics (V_{DS} *vs.* I_{DS}) and (c) the saturation mobility *versus* gate voltage of the **PDPP–TNT** based dual gate OTFT ($L = 50$ μm; $W = 1000$ μm).

and thermal annealing, thin polymer film induces better ordering and improves charge transportation across the channel.[29–31]

High hole mobility, wide absorption in the UV-vis-NIR region, and appropriate HOMO and LUMO energy levels of **PDPP–TNT** are desirable characteristics for an electron donor component in bulk heterojunction solar cells (BHJs). We used **PDPP–TNT** as an electron donor in combination with [6,6]-phenylene-C_{71}-butyric acid methyl ester ($PC_{71}BM$) as an electron acceptor for the fabrication of polymer BHJ solar cells. A solution of **PDPP–TNT** and $PC_{71}BM$ (1 : 2 by weight) in a mixture of chloroform and *o*-dichlorobenzene (4 : 1 by volume) was used to deposit the photoactive layer. **PDPP–TNT** has limited solubility in *o*-dichlorobenzene, so that **PDPP–TNT** readily crystallizes from solution during spin-coating. The best-performing devices were spun from a relatively dilute 15 mg mL^{-1} solution (in comparison, P3HT:PCBM cells are often made from 30 mg mL^{-1} solutions) at a high speed of 5000 rpm. Due to the low vapor pressure of *o*-dichlorobenzene and its preferential PCBM solvation, a PCBM concentration gradient may be induced during spin-coating, *i.e.* the blend film is PCBM-rich towards the cathode, but **PDPP–TNT** rich towards the anode. Such a composition is often beneficial for improving device performance.[37] The inset of Fig. 7a shows the incident photon-to-electron current conversion efficiency (IPCE) spectrum of our best **ITO/PEDOT:PSS/PDPP–TNT:$PC_{71}BM$/Al** solar cell, measured under low-intensity monochromatic light. A photocurrent spectrum is useful to evaluate the ability of a solar cell to convert photons to electrons under irradiation at certain wavelengths and intensities. The shape of the IPCE spectrum was used to calculate a spectral mismatch factor in order to simulate standard AM1.5 conditions. The IPCE spectrum indicates that the active layer is photoactive between 300 and 800 nm which enables higher photon harvesting in the entire visible region. This clearly indicates that in BHJ solar cell devices, the absorption in the long wavelength region is due to the low band gap **PDPP–TNT** polymer whereas absorption in the short wavelength region is mainly from $PC_{71}BM$. Fig. 7a also shows current density–voltage (J–V) curves measured under dark and simulated AM1.5 conditions. The extracted figures-of-merit are: a short-circuit current J_{SC} of 11.8 mA cm^{-2}, open-circuit voltage V_{OC} of 0.76 V, fill factor FF of 0.52 and power conversion efficiency PCE of 4.7%. Higher short circuit current of the OPV devices is due to the low band gap nature and high charge carrier mobility of the polymer. The open circuit voltage value of the device is also quite high, which is due to the lower HOMO energy level of polymer. These results are comparable to those obtained by Janssen *et al.* with PDPTPT.[19]

It is often prudent to calculate a theoretical J_{SC} from the IPCE spectrum and compare it with the actual J_{SC} obtained under simulated AM1.5 conditions to further improve the

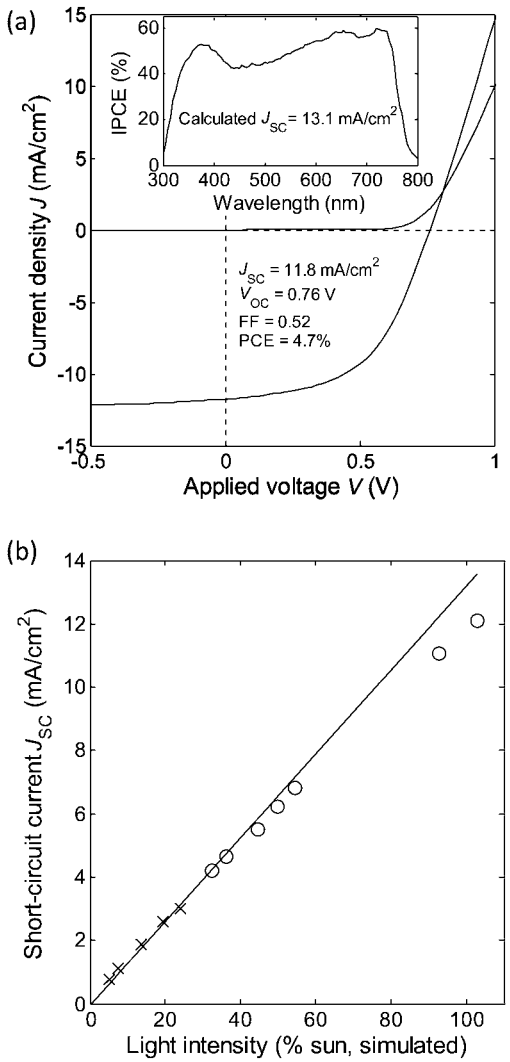

Fig. 7 (a) Current density–voltage curves of the best **PDPP–TNT:PC$_{71}$BM**-based solar cell under dark and simulated AM1.5 conditions. The inset is the incident photon-to-electron current conversion efficiency spectrum under low light intensities. (b) The markers show the variation of J_{SC} with white light intensity between 0.05 and 1.03 suns. The solid line is a linear fit to the first five low-intensity data points (marked by '×'s) and extended into the high-intensity region. The high-intensity data (marked by '○'s) show greater divergence from the linear fit as the light intensity increases.

accuracy of measurement. The two values should match up to verify a correct simulation of AM1.5 conditions. In our measurements, the actual J_{SC} is less than the calculated J_{SC} by about 10%, which is due to our measurement of IPCE under low intensity light. Fig. 7b shows the variation of J_{SC} as white light intensity is increased from 0.05 to 1.03 suns. The solid line is a linear fit to the first five low-intensity data points, which are marked by crosses. At 1 sun, this linear fit passes through 13.2 mA cm^{-2}, which matches well with the J_{SC} value (13.1 mA cm^{-2}) calculated from the IPCE spectrum (see Fig. 7). As intensity increases, the data (circles) diverge from the linear fit, which indicates losses associated with higher photogenerated carrier densities.

Conclusions

In summary, we have reported a novel donor–acceptor solution processable polymer semiconductor **PDPP–TNT** comprised of fused aromatic DPP and naphthalene building blocks in a polymeric backbone. Hole mobilities of 0.65 cm^2 V^{-1} s^{-1} and 0.98 cm^2 V^{-1} s^{-1} were obtained in single and dual gate OTFT device geometries, respectively, with current on/off ratios in the range of 10^5 to 10^7. Such high mobility values are arisen from the strong intermolecular interactions and favorable π–π stacking of fused aromatic DPP–naphthalene conjugated blocks. The OPV devices prepared using **PDPP–TNT** as a donor and PC$_{71}$BM as an acceptor have shown a short-circuit current J_{SC} of 11.8 mA cm^{-2}, open-circuit voltage V_{OC} of 0.76 V, fill factor FF of 0.52, resulting in a power conversion efficiency PCE of 4.7%. **PDPP–TNT** is a versatile donor–acceptor based semiconducting polymer which shows excellent performances in both OTFT and OPV devices. This polymer is a potential candidate for further exploration in various organic electronic devices.

Acknowledgements

The authors thank the Institute of Materials Research and Engineering (IMRE), the Agency for Science, Technology and Research (A*STAR), and the Visiting Investigator Program (VIP) for financial support and Mr Poh Chong Lim for assistance with 2-D XRD. AD and TJH wish to thank CONTACT and NSF-ECCS Division for support of the work at The University of Texas at Austin.

References

1 *Organic Electronics: Materials, Manufacturing, and Applications*, ed. H. Klauk, WILEY-VCH, Weinheim, Germany, 2006.
2 S. Allard, M. Forster, B. Souharce, H. Thiem and U. Scherf, *Angew. Chem., Int. Ed.*, 2008, **47**, 4070–4098.
3 *Organic Photovoltaics*, ed. C. Brabec, V. Dyakonov and U. Scherf, Wiley-VCH, Weinheim, Germany, 2008.
4 K. Müllen and G. Wegner, *Electronic Materials: The Material Approach*, Wiley-VCH, Weinheim, 1998.
5 A. Dodabalapur, *Mater. Today*, 2006, **9**, 24–30.
6 J. Chen and Y. Cao, *Acc. Chem. Res.*, 2009, **42**, 1709–1718.
7 J. Roncali, *Chem. Rev.*, 1992, **92**, 711–738.
8 J. Roncali, *Chem. Rev.*, 1997, **97**, 173–205.
9 B. Tieke, A. R. Rabindranath, K. Zhang and Y. Zhu, *Beilstein J. Org. Chem.*, 2010, **6**, 830–845.
10 M. Zhang, H. N. Tsao, W. Pisula, C. Yang, A. K. Mishra and K. Müllen, *J. Am. Chem. Soc.*, 2007, **129**, 3472–3473.
11 Y. Li, S. P. Singh and P. Sonar, *Adv. Mater.*, 2010, **22**, 4862–4866.
12 Y. Li, P. Sonar, S. P. Singh, M. S. Soh, M. van Meurs and J. Tan, *J. Am. Chem. Soc.*, 2011, **133**, 2198–2204.
13 R. Rieger, D. Bechmann, W. Pisula, W. Steffen, M. Kastler and K. Müllen, *Adv. Mater.*, 2010, **22**, 83–86.
14 L. Bürgi, M. Turbiez, R. Pfeiffer, F. Bienewald, H.-J. Kirner and C. Winnewisser, *Adv. Mater.*, 2008, **20**, 2217–2224.
15 (*a*) I. McCulloch, M. Heeney, C. Bailey, K. Genevicius, I. Macdonald, M. Shkunov, D. Sparrowe, S. Tierney, R. Wagner, W. M. Zhnag, M. L. Chabinyc, R. J. Kline, M. D. Mcgehee and M. F. Toney, *Nat. Mater.*, 2006, **5**, 328–333; (*b*) P. Sonar, S. P. Singh, Y. Li, M. S. Soh and A. Dodabalapur, *Adv. Mater.*, 2010, **22**, 5409–5413.
16 Y. Li, *US Pat.* Application 2009/65766 A1 and 2009/0065878A1, 2009.
17 J. C. Bijleveld, A. P. Zoombelt, S. G. J. Mathijssen, M. M. Wienk, M. Turbiez, D. M. de Leeuw and R. A. J. Janssen, *J. Am. Chem. Soc.*, 2009, **131**, 16616–16617.

18 T. L. Nelson, T. M. Young, J. Liu, S. P. Mishra, J. A. Belot, C. L. Balliet, A. E. Javier, T. Kowalewski and R. D. McCullough, *Adv. Mater.*, 2010, **22**, 4617–4621.
19 J. C. Bijleveld, V. S. Gevaerts, D. D. Nuzzo, M. Turbiez, S. G. J. Mathijssen, D. M. de Leeuw, M. M. Wienk and R. A. J. Janssen, *Adv. Mater.*, 2010, **22**, E242–E246, this paper was published independently while our manuscript was in preparation.
20 M. M. Wienk, M. Turbiez, J. Gilot and R. A. J. Janssen, *Adv. Mater.*, 2008, **20**, 2556–2560.
21 I. McCulloch, M. Heeney, C. Bailey, K. Genevicius, I. Macdonald, M. Shkunov, D. Sparrowe, S. Tierney, R. Wagner, W. M. Zhnag, M. L. Chabinyc, R. J. Kline, M. D. Mcgehee and M. F. Toney, *Nat. Mater.*, 2006, **5**, 328–333.
22 H. Pan, Y. Li, Y. Wu, P. Liu, B. S. Ong, S. Zhu and G. Xu, *J. Am. Chem. Soc.*, 2007, **129**, 4112–4113.
23 J. Li, Q. Fang, Q. Bao, C. M. Li, M. B. Chan Park, W. Zhang, J. Qin and B. S. Ong, *Chem. Mater.*, 2008, **20**, 2057–2059.
24 D. S. Chung, J. W. Park, S. O. Kim, K. Heo, C. E. Park, M. Ree, Y. H. Kim and S. K. Kwon, *Chem. Mater.*, 2009, **21**, 5499–5507.
25 I. McCulloch, C. Bailey, M. Giles, M. Heeney, I. Love, M. Shkunov, D. Sparrowe and S. Tierney, *Chem. Mater.*, 2005, **17**, 1381–1385.
26 B. S. Nehls, PhD thesis, 2005, pp. 1–163.
27 H. Yan, Z. H. Chen, Y. Zheng, C. Newman, J. R. Quinn, F. Dotz, M. Kastler and A. Facchetti, *Nature*, 2009, **457**, 679–686.
28 I. Osaka, T. Abe, S. Shinamura, E. Miyazaki and K. Takimiya, *J. Am. Chem. Soc.*, 2010, **132**, 5000–5001.
29 F. F. Fan, J. Yang, L. Cai, D. W. Price, Jr, S. M. Dirk, D. V. Kosynkin, Y. Yao, A. M. Rawtlett, J. M. Tour and A. J. Bard, *J. Am. Chem. Soc.*, 2002, **124**, 5550–5560.
30 I. Kymissis, C. D. Dimitrakopoulos and S. Purushothaman, *IEEE Trans. Electron Devices*, 2001, **48**, 1060–1064.
31 A. Salleo, M. L. Chabinys, M. S. Yang and R. A. Street, *Appl. Phys. Lett.*, 2002, **81**, 4383–4385.
32 L. Gao, M. A. Peay, D. V. Partyka, J. B. Updegraff, III, T. S. Teets, A. J. Esswein, M. Zeller, A. D. Hunter and T. G. Gray, *Organometallics*, 2009, **28**, 5669–5681.
33 E. Conwell, in *Primary Photoexcitations in Conjugated Polymers: Molecular Excitons* versus *Semiconductor Band Model*, ed. N. S. Sariciftci, World Scientific, Singapore, 1997, ch. 4.
34 Y. Zhu, R. D. Champion and S. A. Jenekhe, *Macromolecules*, 2006, **39**, 8712.
35 H. Sirringhaus, P. J. Brown, R. H. Friend, M. M. Nielsen, K. Bechgaard, B. M. W. Langeveld-Voss, A. J. H. Spiering, R. A. J. Janssen, E. W. Meijer, P. Herwig and D. M. de Leeuw, *Nature*, 1999, **401**, 685–688.
36 S. J. Kim, K. Ryu and S. W. Chang, *J. Mater. Sci.*, 2010, **45**, 566–569.
37 M. Campoy-Quiles, T. Ferenczi, T. Agostinelli, P. G. Etchegoin, Y. Kim, T. D. Anthopoulos, P. N. Stavrinou, D. D. C. Bradley and J. Nelson, *Nat. Mater.*, 2008, **7**, 158–164.

